

# Analytical Evaluation of VCO-ADC Quantization Noise Spectrum Using Pulse Frequency Modulation

Luis Hernandez, *Member, IEEE*, and Eric Gutierrez, *Student Member, IEEE*

**Abstract**—Oversampled ADCs based on voltage-controlled oscillators have been analyzed using statistical models inherited from sigma-delta modulation. This letter shows that the discrete Fourier transform of a VCO-ADC output sequence can be calculated analytically for single tone inputs. The calculation is based on the transformation of the VCO output into a pulse frequency modulated signal that can be represented by a trigonometric series. Knowledge of the VCO-ADC output spectrum allows accurate evaluation of the SNDR dependence with the VCO oscillation frequency and gain constant. The SNDR predictions of the proposed model have been compared to behavioral simulations displaying only a deviation of 0.7 dB.

**Index Terms**—Data conversion, sigma-delta modulation, time encoding, voltage-controlled oscillators.

## I. INTRODUCTION

ONE of the most promising analog-to-digital converter (ADC) architectures nowadays is the VCO-based oversampled converter (VCO-ADC) [1]–[4]. A characterization of its quantization noise spectrum and signal-to-quantization noise ratio (SQNR) would represent a valuable design tool. VCO-ADCs have been described [3], [4] as first-order sigma-delta modulators. Based on these analyses, the SQNR of such converters has been defined for sinusoidal inputs [3], [4] using statistical models for quantization noise. To account for a VCO center frequency different than the sampling rate, [3], [4] show that a DC offset must be added to the input of an equivalent sigma delta modulator. In [5], [6], a formal analysis of a discrete-time first-order sigma-delta modulator showed that its quantization error displays a discrete spectrum.

An analysis based on frequency modulation (FM) seems the natural way to model a VCO-ADC. The spectrum of FM signals for sinusoidal inputs is well known and has been applied to VCO-ADCs in [7]. However, direct application of FM spectral coefficients to a VCO-ADC requires a least-squares minimization technique. In [8], [9] the link between quantization, first-order sigma-delta modulation, and pulse frequency modulation (PFM) was established.

Manuscript received June 12, 2014; revised September 03, 2014; accepted September 07, 2014. Date of publication September 11, 2014; date of current version September 19, 2014. This work was supported by the CICYT project under Grant TEC2010-16330. The associate editor coordinating the review of this manuscript and approving it for publication was Prof. Yiannis Andreopoulos.

The authors are with Carlos III University, Madrid, Spain (e-mail: luish@ing.uc3m.es).

Color versions of one or more of the figures in this paper are available online at <http://ieeexplore.ieee.org>.

Digital Object Identifier 10.1109/LSP.2014.2357071

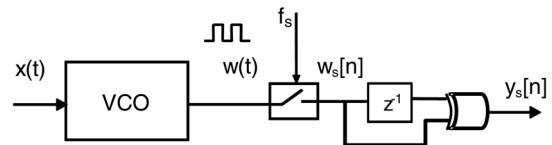


Fig. 1. Block diagram of a single-bit VCO-ADC.

In this letter, we propose an analysis complementary to [3], [4], in which a VCO-ADC is first transformed into a pulse frequency modulator whose spectrum is well known [10]–[12]. This analysis permits to investigate the structure of quantization noise in a VCO-ADC beyond the formal equivalence with a sigma-delta modulator. As a difference to FM, the spectrum of a PFM signal does convey the baseband modulating input signal. The transformation into a PFM brings two advantages. First, the DFT of a finite sequence of a VCO-ADC output can be calculated analytically considering all parameters, such as the VCO center oscillation. This result is not directly provided in [5]. The analytical calculation does not resort to statistical assumptions for quantization noise. Second, the model proposed in this letter does not require expressing the VCO-ADC as a first-order sigma-delta modulator to prove first-order noise shaping. Instead, the VCO-ADC is modeled as a pulse modulation signal coder whose spectral components produce first-order shaped aliases when sampled. This new point of view about VCO-ADCs may extend the research in new data converter topologies [13].

The proposed model allows the evaluation of the peak SQNR and dynamic range of a VCO-ADC at the system level design stage. This analysis is necessary before any other circuit-related consideration such as distortion, thermal noise, or clock jitter. Our analysis will be restricted to sinusoidal inputs, which are the standard test signals used to evaluate ADC parameters.

## II. SYSTEM LEVEL MODEL OF A VCO-BASED ADC

In this section, we will review the model that explains the similarity between a VCO-ADC and a discrete-time sigma-delta modulator, to introduce our model afterwards. Multibit VCO-ADCs use ring oscillators with several phases. We will analyze first a single bit VCO-ADC to extend the results to the multibit case later on.

### A. Classical Analysis of a VCO-ADC

Fig. 1 displays the diagram of a single-bit VCO-ADC.

In Fig. 1, a VCO is modulated by input signal  $x(t)$  defined between  $-1 \leq x(t) \leq 1$ . We will define parameter  $f_v$  as the center oscillation frequency of the VCO ( $x(t) = 0$ ) and parameter  $f_d$  as the VCO frequency gain constant. The sampling frequency for the ADC is  $f_s$ . We will assume the bandwidth of the input

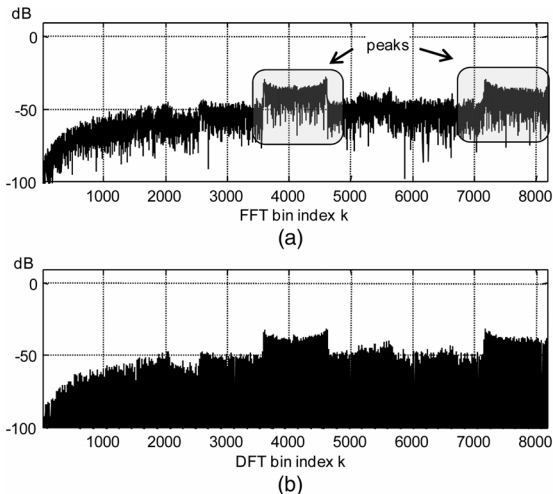


Fig. 2. DFT of  $y_s[n]$  in Fig. 1: (a) simulated, (b) calculated.

signal  $x(t)$  to be much smaller than the center oscillation frequency  $f_v$ . Then, the instantaneous frequency of the oscillator can be written as follows:

$$f(t) = f_v + f_d \cdot x(t) \quad (1)$$

Previous analyses of this architecture [3], [4] use the fact that  $x(t)$  modulates the frequency of the VCO; hence, the VCO phase  $\phi(t)$  represents the integral of  $x(t)$ . In [3], the ADC output ( $y_s[n]$ ) in Fig. 1) is shown to depend on the VCO phase change  $\phi[n]$  and a phase quantization error  $\phi_q[n]$  at the sampling instants:

$$y_s[n] = \frac{1}{2\pi} (\phi[n] + \phi_q[n] - \phi_q[n-1]) \quad (2)$$

Based on the fact that (2) shows a first-order shaped quantization error, most system level analyses [3][4] assume the VCO-ADC to be similar to a discrete sigma-delta modulator. The quantization error of a VCO-ADC has a discrete spectrum that depends on center frequency  $f_v$ . For example, Fig. 2(a) shows a 16k point FFT of  $y_s[n]$  obtained by behavioral simulation in Matlab of Fig. 1, considering  $f_s = 1$ ,  $f_v = f_s/8$ ,  $f_d = f_v/4$ , and a  $-6\text{dB}_{FS}$  input tone at  $f_x = f_s/8192$ . The peaks at high frequency in Fig. 2(a) show that a white spectrum model for quantization noise  $\phi_q[n]$  may not be correct.

### B. Equivalence of a VCO-ADC with a Pulse Frequency Modulator

Fig. 3(a) shows a modification of Fig. 1 where the XOR gate and discrete unit delay have been moved to the left side of the sampler. The discrete unit delay in Fig. 1 has been replaced by a continuous time delay of  $T_s = 1/f_s$  seconds. We will define as  $t_k$  ( $k = 1, 2, \dots, n$ ) the time instants coincident with the edges of  $w(t)$ . We will impose that the minimum time between consecutive edges in  $w(t)$ ,  $T_{\min}$ , is larger than the sampling period  $T_s$ :

$$T_{\min} = \min(t_k - t_{k-1}) \quad T_{\min} > T_s = 1/f_s \quad (3)$$

Otherwise, some edges in  $w(t)$  will not be detected after sampling and the VCO-ADC will not encode the input signal properly. The output signal,  $y_{sa}[n]$  in Fig. 3(a) is equivalent to  $y_s[n]$  in Fig. 1 because the XOR operation may be assumed to be independent of time and the continuous time delay matches with

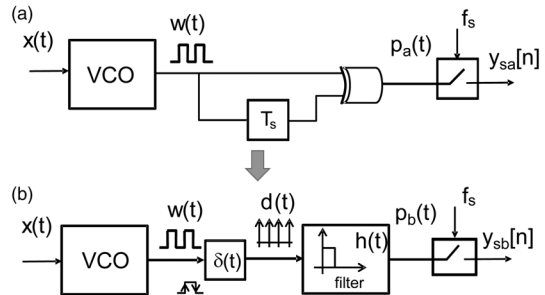


Fig. 3. Transformation of a VCO into a PFM.

one sample delay. This is expressed in the following equation, where  $\otimes$  represents the XOR operation:

$$\begin{aligned} y_s[n] &= w_s[n] \otimes w_s[n-1] & p_a(t) &= w(t) \otimes w(t - T_s) \\ y_{sa}[n] &= p_a(nT_s) = w(nT_s) \otimes w(nT_s - T_s) = y_s[n] \end{aligned} \quad (4)$$

In Fig. 3(a), we define the output of the XOR gate as  $p_a(t)$ , which will be composed of square pulses of constant duration  $T_s$  located at  $t_k$ . The modulation of  $p_a(t)$  is usually referred to as PFM [9]–[12]. Note that the frequency of  $p_a(t)$  is twice that of the VCO because both rising and falling edges in  $w(t)$  produce a pulse in  $p_a(t)$ . Therefore, we will define the pulse frequency as  $f_o = 2f_v$ .

We may propose a further equivalent system to Fig. 3(a). In Fig. 3(b), we have replaced the delay and XOR gate of Fig 3(a) by a filter with square impulse response  $h(t)$  of duration  $T_s$  that is driven by signal  $d(t)$ . Signal  $d(t)$  will have a Dirac delta at times  $t_k$ . Signal  $p_b(t)$  in Fig. 3(b) will be the output of the filter and can be computed as follows:

$$\begin{aligned} d(t) &= \sum_{k=0}^{\infty} \delta(t - t_k) & p_b(t) &= h(t) * d(t) \\ & & &= \sum_{k=0}^{\infty} u(t - t_k) - u(t - t_k - T_s) \end{aligned} \quad (5)$$

Therefore,  $p_a(t) = p_b(t)$  and  $y_{sa}[n] = y_{sb}[n] = y_s[n]$  in Fig. 1, Fig. 3(a), and Fig. 3(b). The model of Fig. 3(b) reveals that filter  $h(t)$  will shape the spectrum of  $p_b(t)$ . The transfer function of this filter,  $H(\omega)$ , will be a sinc function whose zeroes are located at integer multiples of  $f_s$ .

### C. Spectral Analysis Of A Pulse Frequency Modulator

The spectrum of pulse modulations was analyzed at the beginning of digital communications. In particular, a trigonometric series expansion for a PFM signal having a center frequency  $f_o$  and linear FM (1) was calculated in [10][11] for sinusoidal inputs  $x(t)$  of the form:

$$x(t) = A \cdot \cos(\omega_x t) \quad \omega_x = 2\pi f_x, A \leq 1 \quad (6)$$

Signal  $p_b(t)$  in Fig. 3(b) corresponds to this class of modulations. Knowledge of a trigonometric series expansion of  $p_b(t)$  permits calculation of its Fourier transform,  $P_b(\omega)$ , which will be a sum of Dirac delta functions. Once  $P_b(\omega)$  is known, we may calculate the DFT of  $y_{sb}[n]$  in Fig. 3(b) that will be coincident with the DFT of  $y_s[n]$  in Fig. 1. An analytical representation of the DFT of  $y_s[n]$  allows prediction of the spectrum and SQNR of an ideal VCO-ADC without resorting to simulation.

#### D. Oscillator Spectrum Before Sampling

According to [10], signal  $p_b(t)$  in Fig. 3(b) can be expanded into the following trigonometric series:

$$\begin{aligned}
 f_o &= 2f_v, \quad \omega_o = 2\pi f_o \\
 p_b(t) &= DC + BB \cdot \cos(\omega_x(t - T_s/2)) \\
 &+ \sum_{q=1}^{\infty} \sum_{r=-\infty}^{\infty} CH(q, r) \cdot \cos((q\omega_o + r\omega_x) \cdot (t - T_s/2)) \\
 DC &= T_s \cdot f_o, \quad BB = \frac{Af_d}{\pi f_x} \cdot \sin(\omega_x \cdot T_s/2) \\
 CH(q, r) &= 2J_r(q \frac{Af_d}{f_x}) \cdot \frac{\sin((q \cdot \omega_o + r \cdot \omega_x) \cdot T_s/2)}{\pi \cdot q}
 \end{aligned} \quad (7)$$

In (7),  $J_r$  is the  $r$ th order Bessel function of the first kind. This series contains a constant component (DC) and a baseband component (BB) representing the input signal. Coefficients  $CH(q, r)$  represent the amplitudes of the harmonics of the center frequency  $f_o$ , and sideband tones around such harmonics. Integer  $q$  indexes the harmonics of  $f_o$  and integer  $r$  indexes the sideband tones around each harmonic at  $qf_o$ . The sinc transfer function corresponding to filter  $h(t)$  in Fig. 3(b) is reflected into coefficient  $CH(q, r)$ , which is zero at integer multiples of  $f_s$ . The attenuation and phase shift of  $x(t)$  due to  $h(t)$  are also reflected in BB.

The Fourier transform  $P_b(\omega)$  will be a sum of Dirac deltas weighted by the coefficients expressed in (7):

$$\begin{aligned}
 P_b(\omega) &= 2\pi \cdot DC \cdot \delta(\omega) \\
 &+ \pi \cdot BB \cdot \left( e^{\frac{j\omega_x T_s}{2}} \delta(\omega + \omega_x) + e^{-\frac{j\omega_x T_s}{2}} \delta(\omega - \omega_x) \right) \\
 &+ \sum_{q=1}^{\infty} \sum_{r=-\infty}^{\infty} \pi \cdot CH(q, r) \\
 &\cdot \left( e^{\frac{j(q\omega_o + r\omega_x)T_s}{2}} \delta(\omega + (q\omega_o + r\omega_x)) \right. \\
 &\left. + e^{-\frac{j(q\omega_o + r\omega_x)T_s}{2}} \delta(\omega - (q\omega_o + r\omega_x)) \right)
 \end{aligned} \quad (8)$$

We have represented in Fig. 4(b) part of the modulus of  $P_b(\omega)$  predicted by (8) with the same parameters defined for the simulation of Fig. 2(a). The modulus of  $H(\omega)$  is also represented in Fig. 4(b) as a dotted line. We have marked the tones weighted by  $CH(q, r)$  corresponding to the sidebands of the first three harmonics of  $f_o$ . The harmonic sidebands represented by  $CH(q, r)$  occupy a bandwidth that increases with  $q$  and whose average level decays with  $q$ . After some harmonics, the sidebands overlap resembling a noise shaped by  $H(\omega)$ .

We may also observe in Fig. 4(b) the gap between the center frequency sidebands and DC, inside of which the sideband energy is small. If the input analog band width (ABW) of the ADC fits in this gap, the input signal will be encoded in  $p_b(t)$  with nearly no error.

As a comparison, Fig. 4(a) represents the modulus of  $P_b(\omega)$  plotted with data from the behavioral simulation of Fig. 2(a).

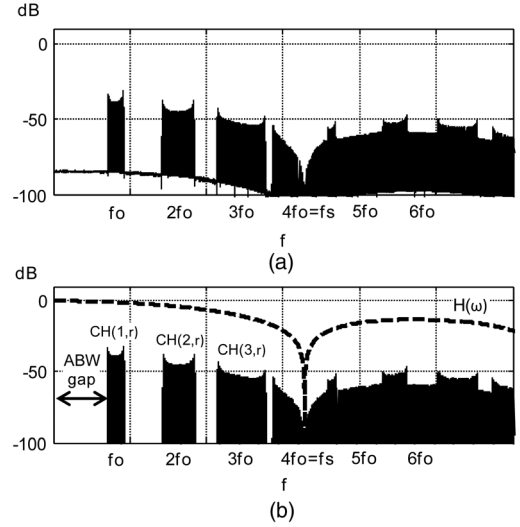


Fig. 4. Modulus of  $P_b(\omega)$  (a) simulated, (b) calculated.

In Fig. 4, we may observe the agreement of the simulated and calculated values of  $P_b(\omega)$  and also the nulls imposed by  $H(\omega)$ .

#### E. Sampled Spectrum

Our interest in the system of Fig. 1 is to obtain a sampled sequence of integer values that may represent  $x(t)$ . Therefore, we predict the DFT of a finite set of  $N$  samples of  $y_s[n]$  ( $N$  even), as is usually done to evaluate the performance of an ADC. This DFT can be calculated if the input tone at  $f_x$ , the sampling frequency  $f_s$ , the center frequency  $f_o$ , and the sequence length  $N$  are all linked by integer factors  $K_s$ ,  $K_o$ , and  $K_x$  as follows:

$$f_s = 2K_s \cdot f_x, \quad f_o = K_o \cdot f_x, \quad N = 2K_x K_s \quad (9)$$

These definitions force all tones in the spectrum of  $p_b(t)$  to fit into a bin of the DFT of  $y_s[n]$ . All DFT bins that are not an integer multiple of  $K_x$  will be zero. Therefore, the DFT of  $y_s[n]$  may be indexed by an integer  $k$  ( $k = 0, 1, 2, \dots$ ) multiplied by  $K_x$ . In practice,  $f_x \ll f_o$  and we may find an integer  $K_o$  that closely approximates the desired  $f_o$ .

We may evaluate  $Y[kK_x]$ , the DFT of  $y_s[n]$ , using the coefficients of  $P_b(\omega)$ . A delta located at frequency  $\omega$  in  $P_b(\omega)$  will alias to DFT bin  $kK_x$  as follows:

$$\begin{aligned}
 \omega(q, r) &= q\omega_o + r\omega_x = q\omega_x K_o + r\omega_x \\
 k &= \text{mod}(qK_o + r, 2K_s), \quad k = 0 \dots 2K_s - 1
 \end{aligned} \quad (10)$$

In (10),  $\text{mod}$  represents the remainder of integer division by  $2K_s$ . To calculate DFT bin  $kK_x$ , it suffices to add all the complex coefficients of the Dirac deltas in  $P_b(\omega)$  that alias to that particular index  $k$ . Let  $R(k)$  be the set of all pairs  $(q, r)$  of integers complying with condition (10). The values of  $Y[kK_x]$  are calculated in (11). To calculate  $Y[kK_x]$ , we have approximated the DFT bins of the DC component and input signal component BB neglecting the contributions of the center frequency harmonic

sideband aliases due to their proximity to the nulls of sinc function  $H(\omega)$ .

$$\begin{aligned}
 R(k) &= \{q \in \{1..\infty\}, \\
 & r \in \{-\infty..\infty\} / k = \text{mod}(qK_0 + r, 2K_s)\} \\
 Y[0] &\cong T_s f_0 \quad BB = \frac{Af_d}{\pi f_x} \cdot \sin\left(\frac{\pi}{2K_s}\right) \\
 CH(q, r) &= \frac{2}{\pi q} J_r\left(q \frac{Af_d}{f_x}\right) \cdot \sin\left((qK_0 + r) \frac{\pi}{2K_s}\right) \\
 Y[K_x] &\cong BB \cdot e^{-j \frac{\pi}{2K_s}}, \quad Y[N - K_x] \cong BB \cdot e^{j \frac{\pi}{2K_s}} \quad (11) \\
 Y[kK_x] &= \sum_{R(k)} CH(q, r) \cdot e^{-j \frac{\pi}{2K_s}(qK_0 + r)} \\
 /k &= \text{mod}(qK_0 + r, 2K_s), \quad 2 \leq k \leq K_s - 1 \\
 Y[kK_x] &= \sum_{R(k)} CH(q, r) \cdot e^{j \frac{\pi}{2K_s}(qK_0 + r)} \\
 /k &= \text{mod}(qK_0 + r, 2K_s), \quad K_s \leq k \leq 2K_s - 2
 \end{aligned}$$

We have applied (11) to reproduce the simulation in Fig. 2(a) by analytical calculation of  $Y[k]$ . The result is shown in Fig. 2(b), which replicates the peaks and shape of Fig. 2(a).

These results can be extended to a multibit VCO-ADC. A VCO with  $M$  phases can be assumed equivalent to a single bit VCO with a center frequency  $M$  times higher. To model a multibit VCO-ADC we may still use the model of Fig. 3(b) using a rest frequency  $f'_{v,n} = Mf_v$  but keeping  $T_s$  as the duration of the impulse response of  $h(t)$ . In the multibit case, (3) will no longer hold as there may be more than one delta pulse per sampling period  $T_s$  in  $d(t)$ . The square pulses at  $p(t)$  in Fig. 3(b) will overlap forming a multilevel signal. The PFM spectrum calculated in [11] refers to the delta pulse signal  $d(t)$  in Fig. 3(b). The inclusion of the square pulse shaping filter  $h(t)$  in [10] only introduces a sinc filtering in the spectrum over the series expansion calculated in [11]. Therefore, (8) and (11) may be used regardless that the pulses overlap or not.

### F. SQNR Prediction

Equation (11) describes the spectrum of  $y_s[n]$  and hence, it is possible to predict the SQNR of the ADC. For this purpose, we only need to calculate the DFT bins of  $Y[kK_x]$  that lie inside the ABW defined by the sampling frequency and the oversampling ratio (OSR). We may define index  $k_{ABW}$  as the closest DFT bin index corresponding to the edge of the ABW. Then, the value of the SQNR will be:

$$\begin{aligned}
 k_{ABW} &= \text{int}\left(\frac{K_s}{OSR}\right), \\
 SQNR(dB) &= 10 \log_{10} \frac{|Y[K_x]|^2}{\sum_{k=2}^{k_{ABW}} |Y[kK_x]|^2} \quad (12)
 \end{aligned}$$

Observing (11), we see that each set  $R(k)$  contains an infinite number of values of  $q$  and  $r$ . However,  $CH(q,r)$  quickly decreases away from the center frequency harmonics, as shown in Fig. 4. Therefore, to practically calculate (12), we may define some bounds for  $q$  and  $r$  to truncate the summation. A simple algorithm to calculate the SQNR is described next. Coefficients  $Y[kK_x]$  can be computed by adding all the tone complex coefficients (11) that alias to DFT bin  $kK_x$ . We will establish a noise floor  $Y_{ref}$  below in which a term  $CH(q,r)$  in (7) can be discarded.

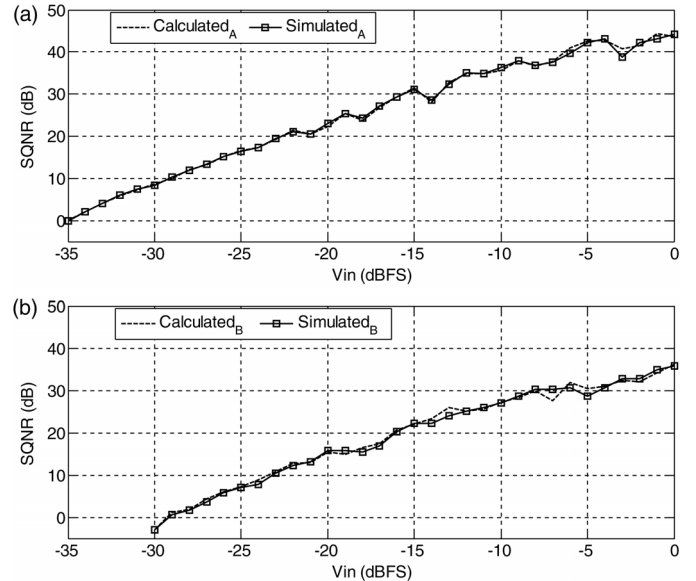


Fig. 5. Dynamic range comparison: (a)  $f_v = f_s/8$ ,  $f_d = f_s/16$ ,  $f_x = f_s/8192$ ; (b)  $f_v = f_s/16$ ,  $f_d = f_s/64$ ,  $f_x = f_s/4096$ .

As larger values of  $CH(r,q)$  correspond to smaller values of  $q$ , we will start at  $q = 1$  and sweep index  $r$ . When  $Y_{ref}$  reaches in the computation of  $CH(q,r)$ , we no longer need to increase  $r$  further and can jump to the next value of  $q$ . If the resulting index  $k$  (10) is above  $k_{ABW}$ , it can be discarded, which significantly speeds the computation of SQNR.

Fig. 5 shows a comparison between the dynamic ranges obtained by the behavioral simulation of Fig. 2(a) (simulated SQNR) and the proposed method (calculated SQNR), considering an OSR = 64 and  $f_s = 1$ . In Fig. 5, two cases have been plotted (5.a and 5.b) to evaluate different center oscillation frequencies  $f_v$ , VCO gain constants  $f_d$ , and input tone frequencies  $f_x$ . The SQNR calculations were performed with 32k point FFTs and  $Y_{ref} = -150\text{dB}_{FS}$ . The simulations deviate from the analytical calculations in less than 0.7 dB.

### III. CONCLUSIONS

In this letter, we have discussed the analogy between a VCO-ADC and a pulse frequency modulator. This analogy allows analytical calculation of the DFT of the output sequence and expected SQNR of the converter for single tone inputs. This modeling takes into account parameters such as center oscillation frequency and gain constant of the VCO. The mathematical derivations have been verified by evaluating the dynamic range of a VCO-ADC example by calculations and by a behavioral simulation, achieving a 0.7 dB mismatch.

In addition, the model of a VCO-ADC proposed here shows an alternative explanation for noise shaping in which discretization and quantization of the VCO phase are not required. Instead, the model shows that the VCO acts as an analog pulse frequency signal coder (similar to other pulse-coded modulators such as PWM, PDM, etc.) [7]. This is shown in the example of Fig. 4, where a low-frequency input signal is encoded with nearly no error in a narrow band. Quantization error is generated afterwards by aliases produced by sampling. Therefore, the noise-shaping effect seems to depend on the square pulse embedded in the post processing of the VCO output. This different point of view allows devising other data-converter topologies [13].

## REFERENCES

- [1] M. Hovin, A. Olsen, T. S. Lande, and C. Toumazou, "Delta-sigma modulators using frequency-modulated intermediate values," *IEEE J. Solid-State Circuits*, vol. 32, no. 1, pp. 13–22, Jan. 1997.
- [2] J. Daniels, W. Dehaene, M. Steyaert, and A. Wiesbauer, "A 0.02 mm<sup>2</sup> 65 nm CMOS 30 MHz BW all-digital differential VCO-based ADC with 64 dB SNDR," in *IEEE Symp. VLSI Circuits (VLSIC)*, 2010, Jun. 16–18, 2010, pp. 155–156.
- [3] J. Kim, T.-K. Jang, Y.-G. Yoon, and S. H. Cho, "Analysis and design of voltage-controlled oscillator based analog-to-digital converter," *IEEE Trans. Circuits Syst. I*, vol. 57, no. 1, pp. 18–30, Jan. 2010.
- [4] G. Taylor and I. Galton, "A mostly-digital variable-rate continuous-time delta-sigma modulator ADC," *IEEE J. Solid-State Circuits*, vol. 45, no. 12, pp. 2634–2646, Dec. 2010.
- [5] R. M. Gray, W. Chou, and P. W. Wong, "Quantization noise in single-loop sigma-delta modulation with sinusoidal inputs," *IEEE Trans. Commun.*, vol. 37, no. 9, pp. 956–968, Sep. 1989.
- [6] N. T. Thao, "Formal spectral theory for ideal sigma-delta quantization with stationary time-varying inputs," in *IEEE Int. Conf. Acoustics, Speech and Signal Processing, 2007 ICASSP*, Apr. 15–20, 2007, vol. 3, pp. III-1481–III-1484.
- [7] T. Redant, P. A. J. Nuyts, P. Reynaert, and W. Dehaene, "Presilicon circuit-aware linear least squares spectral analysis for time-based data converters," *IEEE Trans. Circuits Sys. II: Exp. Briefs*, vol. 60, no. 11, pp. 751–755, Nov. 2013.
- [8] C. M. Zierhofer, "Frequency modulation and first-order delta sigma modulation: Signal representation with unity weight Dirac impulses," *IEEE Signal Process. Lett.*, vol. 15, pp. 825–828, 2008.
- [9] C. M. Zierhofer, "Quantization noise as superposition of frequency-modulated sinusoids," *IEEE Signal Process. Lett.*, vol. 16, no. 11, pp. 933–936, Nov. 2009.
- [10] E. Fitch, "The spectrum of modulated pulses," *J. Inst. Elect. Eng. III: Radiocommunication*, vol. 94, no. 13, pp. 556–564, Mar.–Apr. 1947.
- [11] E. J. Bayly, "Spectral analysis of pulse frequency modulation in the nervous systems," *IEEE Trans. Biomed. Eng.*, vol. BME-15, no. 4, pp. 257–265, Oct. 1968.
- [12] B. Wilson, F. Ghassemlooy, and L. Chao, "Squarewave frequency modulation techniques," *IEEE Trans. Commun.*, vol. 43, no. 234, pp. 1505–1512, Feb./Mar./Apr. 1995.
- [13] L. Hernández and E. Gutiérrez, "Oversampled ADC based on pulse frequency modulator and TDC," *Electron. Lett.*, vol. 50, no. 7, pp. 498–499, Mar. 2014.